Energy Reports 11 (2024) 1242–1255

Contents lists available at ScienceDirect

Energy Reports

journal homepage: www.elsevier.com/locate/egyr

Research paper

Parametric comparison of a CPVT performance evaluation under standard testing procedures - ISO 9806:2017 and IEC 62108:2016 - for an automated and manual 2-axis tracking solar system stand

Diogo Cabral [a,*], George Kosmadakis [b], Emmanouil Mathioulakis [b]

[a] Department of Building Engineering, Energy Systems and Sustainability Science, University of Gävle, Kungsbäcksvägen 47, 801 76 Gävle, Sweden
[b] Solar & Other Energy Systems Laboratory, National Centre for Scientific Research "Demokritos", Agia Paraskevi, Greece

ARTICLE INFO

Keywords:
Symmetric C-PVT collector
STC testing conditions
ISO 9806:2017
IEC 62108:2016

ABSTRACT

Currently, a noticeable lack of literature with respect to a wide-ranging comparison of the precision exhibited by automated and manual two-axis tracking solar systems, particularly within the context of adhering to the standard testing protocols delineated by ISO and IEC. To address this research gap, a symmetrical concentrating Photovoltaic-Thermal solar collector underwent a detailed evaluation encompassing two standard testing procedures such as ISO 9806:2017 and IEC 62108:2016. This comprehensive assessment covered thermal and electrical performance parameters, unfolding across two distinct geographical locations: Athens (Greece) and Gävle (Sweden). Within this experimental framework, an automated two-axis tracking solar system stand was employed at the Greek testing site, while in Sweden it was characterized by the employment of a manual two-axis tracking solar system. The collective peak power performance presented marginal divergence within a narrow range of $\pm$ 1% across both testing sites. This culminated in an overall peak power output of 1550 W_{peak}, which included an electrical peak capacity of 218 W_{peak} and a thermal peak power of approximately 1332 W_{peak}. Notably, the most pronounced deviation has been materialized in the transversal and longitudinal Incidence Angle Modifier coefficients, with disparities remaining limited to a threshold of $< 5\%$. These findings underscore the commendable precision hallmarking. In summary, the outcomes presented in this study not only contribute to the extant body of knowledge by bridging the existing gap in literature, but also emphasize the precision inherent to manual two-axis tracking solar systems when compared with automated equivalents.

1. Introduction

A salient advantage of solar energy technologies, encompassing PV, Solar Thermal (ST), and more recently Photovoltaic-Thermal (PVT) systems, resides in their capability to harvest electricity or heat precisely at sites of optimal convenience, such as industrial or residential structures (Chakravarty et al., 2022). PVT systems, specifically, capitalize on surplus heat from PV cells to generate valuable thermal energy, simultaneously augmenting the electrical efficiency within the same spatial footprint. This innovative approach amplifies installation capacity within constrained areas. Consequently, end-users have the capacity to generate their own energy for heating and cooling purposes, thereby mitigating their environmental impact (Zhang et al., 2022) through localized energy production.

Furthermore, electricity generation via solar systems is facilitated through diverse methodologies, including PV, ST, concentrating solar-thermal power (CSP) systems, and more recently, concentrating Photovoltaic-Thermal (CPVT) configurations. The latter, CPVT, stands out for its ability to optimize energy output in terms of both heat and electricity within confined installation areas (Cabral, 2022).

1.1. Knowledge gap

The requirements to achieve better precision while testing solar collectors under different standard testing procedures such as ISO and IEC, typically lead researchers to opt from the conventional manual 2-axis trackers for more complex and expensive automated 2-axis trackers.

Although both types of 2-axis solar trackers aim to keep the solar collector perpendicular to the sun's rays, there are some differences in their operation, and several peer-reviewed articles such as El Hammoumi et al. (2022); Tina and Scavo (2022); Vargas et al. (2022) and

* Corresponding author.
E-mail address: diogo.cabral@hig.se (D. Cabral).

https://doi.org/10.1016/j.egyr.2023.12.069
Received 29 August 2023; Received in revised form 25 November 2023; Accepted 30 December 2023
Available online 9 January 2024

Nomenclature

Symbol	Description [Unit]
θc	Acceptance half-angle [°]
ta	Ambient temperature [°C]
Gb	Beam irradiance [W/m2]
tcell,PVT	Cell temperature [°C]
Ci	Concentration factor [−]
b0	Constant for incident angle modifier
Gd	Diffuse irradiance [W/m2]
c5	Effective thermal capacity [J/m2. K]
Ks	Effective thermal conductivity [W/m.K]
ηel,STC	Electrical efficiency at standard testing conditions [−]
a1	Heat loss coefficient at (tm − ta) = 0 [W/m2. K]
θ	Incidence angle [°]
Kθb(θL,θT)	Incidence angle modifier for beam radiation [−]
Kθd	Incidence angle modifier for diffuse radiation [−]
t_r	Light transmission [−]
tm	Mean fluid temperature [°C]
η0,b	Peak collector efficiency at ΔT = 0 K [−]
a8	Radiation losses [W/m2. K4]
c4	Sky temperature dependence of heat loss coefficient [−]
G	Solar irradiance [W/m2]
P_{el}	Specific electrical power output [W/m2]
Q_{th}	Specific thermal power output [W/m2]
u	Surrounding air speed [m/s]
β	Temperature coefficient of electrical power [%/K]
a2	Temperature dependence of heat loss coefficient [W/m2. K2]
U	U-value
U0	U-value at optical efficiency
a7	Wind dependence of IR radiation exchange [W/m2. K4]
a6	Wind dependence of the zero-loss efficiency [s/m]
a3	Wind speed dependence of heat loss coefficient [J/m3. K]

Subscripts

BEMS	Building Energy Management System
BIPV	Building Integrated Photovoltaic
BTES	Borehole Thermal Energy Storage
CPC	Compound Parabolic Collector
CPVT	Concentrating Photovoltaic-Thermal
DAT	Dual Axis Tracker
DNI	Direct Normal Irradiation
DHW	Domestic Hot Water
FAT	Fixed Axis Tracker
HSAT	Horizontal Single Axis Tracker
HT	Heat Pump
HTF	Heat Transfer Fluid
IAM	Incidence Angle Modifier
LCPVT	Low Concentrating Photovoltaic-Thermal
O&M	Operation & Maintenance
PV	Photovoltaic
PVT	Photovoltaic-Thermal
QDT	Quasi Dynamic Testing
R&D	Research & Development
ST	Solar Thermal
VSAT	Vertical Single Axis Tracker

Demirdelen et al. (2023) address these differences, focusing their studies on energy yield assessment.

The above-mentioned research articles provide evidence that by comparing the energy yield provided by manual and automated 2-axis trackers, the latter achieves higher efficiency and accuracy in harvesting solar energy. On the other hand, no peer-reviewed literature focuses solely on comparing both technologies for different thermal and electrical parameter assessments (e.g., for certification purposes), as required by the ISO and IEC standards.

Therefore, this manuscript aims at filling the knowledge gap that currently exists between testing solar collectors with automated and manual 2-axis solar trackers, providing research & development (R&D) institutes with different options with lower maintenance and thus more affordable testing method procedures.

Typically, for assessing specific electrical and thermal parameters it is required an automated 2-axis tracker as it typically uses sensitive equipment and mechanical bodies to continuously adjust the position of the solar collector, while manual 2-axis trackers require manual adjustment. Demirdelen et al. (2023) presented a study focused on an electrical energy yield assessment made by automated 2-axis trackers, which concluded that this technology is generally more efficient in their operation as it tracks the sun more accurately than a manual 2-axis tracker.

In contrast, the general perception is that manual 2-axis trackers require more effort and are less precise than automated 2-axis trackers. In reality, there is still no clear understanding of their comparative efficiency when applied to testing standards of solar collectors as ISO or IEC for their both electrical and thermal parameters, which this manuscript addresses and demystifies.

Additionally, these systems are typically less expensive due to fewer electronic components, and the Operation & Maintenance (O&M) is considerably lower than automated 2-axis trackers, which tend to have higher tracking accuracy, thus harvesting more efficiently the sunlight, due to real-time monitoring and adjustment capabilities. Nevertheless, the higher 'theoretical' precision (which increases costs and will be addressed in this manuscript) affects maintenance needs, requiring more maintenance due to complex electronic components (Tajouo et al., 2023), while manual systems rely on manual adjustments.

Moreover, the automated 2-axis trackers have (i) higher tracking accuracy, (ii) potential for integration with smart grids and energy management systems, (iii) better 'theoretical' performance in varying weather conditions when applied in PV fields. On the other hand, the (i) higher initial and O&M costs, (ii) the dependence on electronics and sensors, and the (iii) potential for system downtime, if components fail, comprise its disadvantages.

Conversely, the manual 2-axis trackers have (i) lower upfront costs, (ii) simpler design, (iii) potential for reduced maintenance costs, (iv) suitable for small-scale or remote applications where automation is impractical while having (i) Lower tracking accuracy (when applied in PV fields), (ii) a dependence on human intervention, (iii) reduced performance during cloudy or fluctuating weather conditions.

Furthermore, there is little research on the long-term maintenance requirements of automated 2-axis trackers compared to manual 2-axis trackers, thus requiring additional research to assess which type of tracker is the most efficient and reliable for testing solar collectors.

To tackle the before-mentioned topics of interest, this manuscript presents a set of electrical and thermal outdoor testing results for two different locations, Gävle (Sweden) and Athens (Greece), under the ISO 9806: (2017) (e.g., thermal assessment) and 62108:2016 (e.g., electrical assessment). The solar collector parameters were retrieved by performing both electrical/thermal longitudinal/transversal Incidence Angle Modifier tests, as well as daily electrical/thermal peak/efficiency performance assessments. The developments made by Cabral (2022) comprised mainly solar collector construction, therefore, this manuscript focused on the further improvement of the solar collector, developed by Cabral (2022), through better thermal insulation (e.g., all

the joints were properly sealed), which will lead to a lower thermal loss coefficient and a more compact prototype.

The measurement sets were retrieved by following the standard testing procedures, ISO 9806: (2017) and IEC 62108: (2016) (presented in the following chapter 1.2), where the Greek outdoor test was performed with an automated 2-axis tracking system, whereas the Swedish outdoor testing procedure was performed with a manual 2-axis tracking solar system. This was aimed to assess the real difference between these two solar testing stands in terms of effective efficiency and the need for solar R&D institutes to invest in high maintenance and cost investment of automated 2-axis solar tracking system stands.

1.2. Solar tracking systems

PV modules are typically mounted on a wide-open area to harvest the sunlight. To increase/maximize solar radiation, typically the PV modules are typically installed in solar tracking systems. Solar trackers are typically divided into 4 main categories (Dekkiche et al., 2023), such as:

- Fixed Axis Tracker (FAT) – Fixed position.
- Horizontal Single Axis Tracker (HSAT) – Fixed azimuth at 0º.
- Vertical Single Axis Tracker (VSAT) – Rotates around the vertical axis.
- Dual Axis Tracker (DAT) – rotates around both vertical and horizontal axis.

These systems can be further utilized for either daily or seasonal tracking modes (Asfaw, 2023). The 1-axis tracking modes (i.e., daily, or seasonal), can be further detailed into an east-west daily tracking mode or north-south seasonal tracking mode, whereas the 2-axis tracking system is able to do both, which maximizes the harvesting of the available sunlight that falls into the solar collector plane.

On the other hand, when both tracking systems (i.e., HSAT, VSAT and DAT) are in automatic mode, it requires a gear, a power source and a pyrheliometer (e.g., a solar device that follows the sun and keeps the solar collector plane perpendicular to the sun rays), which increases complexity and maintenance/capital costs, when compared with a manual tracking solar system. Regarding the capital costs of the above-mentioned 4 tracking systems, the FAT is considered to have a negligible cost, whereas the HSAT, VSAT and DAT are typically in the range of 870, 255 and 1000 $/kW, respectively (Dekkiche et al., 2023).

1.3. Reflector geometry concept overview

Coupling PV cells with solar thermal absorbers rises challenges regarding the amount and uniformity of sunlight onto the PV cells. This leads to higher precision reflector geometries to ensure the highest light uniformity possible, therefore the studied CPVT solar collector has been designed to tackle these challenges, which can be found in more detail at Cabral (2022).

Moreover, by implementing solar reflectors, the sunlight is focused onto a small area (e.g, receiver), providing a practical approach to generate thermal energy at higher temperatures and therefore with higher potential value. Additionally, concentration on PVTs decreases the amount of PV cells needed, thus lowering the solar collector manufacturing cost (e.g., reduction in material such as selective surface or solar PV cells). These solar collectors require a lower receiver area, which decreases the heat loss area (e.g, thus the heat loss coefficient) while enhancing the annual energy yield performance (Cabral et al., 2019). On the other hand, decreasing the overall size of the receiver will also impact negatively the Incidence Angle Modifier (IAM) due to higher reflection losses.

Furthermore, the PV cell sub-string (i.e, total length of 2100 mm) has been encapsulated in a silicone gel from Wacker-Elastolsil Solar 2205, with a 0.2 W/m.K thermal conductivity and light transmittance of around 97%. The PVT absorber, with 2310 mm of length, 165 mm of width and thickness (r) of around 14.5 mm, is equipped with 8 elliptical channels to enhance the heat transfer between the aluminium receiver core and the Heat Transfer Fluid (HTF). The low iron solar glass (from Scheuten Glas) is characterised by an emissivity of 84%, a thickness of 4 mm, a thermal conductivity of 1 W/m.K and a transmittance of 91 $\pm$ 0.5%. The following Table 1 presents a summary of the main parameters that characterize the PV cells used in the PCVT solar collector presented in this manuscript.

To reduce the series resistances, the PV cells have been cut to three-quarters-size PV cells, which will lead to a theoretical maximum output power P_{mpp} and short-circuit current I_{sc} be equal to a one-third-size PV cell performance, while the open-circuit voltage V_{oc} remains unchanged.

2. International certification standards for parameter characterization and testing facilities description

2.1. IEC 62108:2016 Testing Standard

The IEC 62108:2016 - Concentrator Photovoltaic (CPV) Modules and Assemblies - Design Qualification and Type Approval - international standard specifies the minimum requirements for the design qualification and type approval of concentrator photovoltaic (CPV) modules and assemblies suitable for long-term operation in general open-air climates as defined in IEC 60721–2-1. The test procedure is partially based on that specified in IEC 61215–1.

The standard tends to assess the electrical, mechanical, and thermal characteristics of the CPV modules, as well as proving the capability of concentrating solar technologies of withstanding prolonged exposure in climates described within a specific scope, which comprises the following main technical changes from the previous revision of this standard:

- changes in outdoor exposure from 1000 h to 500 h;
- changes in current cycling during the thermal cycling test;
- added dust ingress test;
- eliminated thermal cycling associated with damp heat test;
- eliminated UV exposure test.

2.2. ISO (9806): (2017) Testing Standard

The ISO, 9806:, 2017 standard focuses on the assessment of thermal performance, safety, durability and reliability testing of solar collectors that are available or almost ready to go into the market. ‘The standard applies to liquid heating collectors, air heating collectors, hybrid solar collectors co-generating heat and electric power (e.g., PVTs), as well as to solar collectors using external power sources for normal operation and/or safety purposes (e.g., tracking concentrating collectors)’ (ISO, 9806:, 2017). All the required testing procedures to assess the performance of solar collectors that co-generate heat and electrical power such as PVTs shall:

- be made under maximum electrical power point conditions (MPPT-Mode);
- for all durability tests, the electrical power shall not be connected to any load (open circuit) to prevent cooling and to simulate worst-case operating conditions.

On the other hand, the standard does not offer a testing procedure for

Table 1
Summary of the main parameters that characterize the PV cells.

Efficiency [%]	P_{mpp} [W]	V_{mpp} [V]	I_{mpp} [A]	V_{oc} [V]	I_{sc} [A]	Temperature coefficient [%/ºC]
20.1	1.57	0.53	2.96	0.63	3.13	-0.37

electrical safety, as ISO (9806): (2017) has been initially developed to assess the thermal behaviour of thermal collectors and not hybrid/PV solar collectors. This manuscript focuses solely on the electrical performance testing procedure of the IEC 62108:2016 for both automated and manual 2-axis solar tracking systems. Despite the new updates implemented in the IEC 62108:2016 to create the newest IEC 62108:2022, this manuscript is based on the IEC 62108:2016.

2.3. Description testing the PVT collector

The report presents the testing facilities and the main test data that have been obtained. The testing protocol of the thermal properties followed the procedures of the ISO (9806): (2017) standard (Solar Keymark), expanding where necessary the testing conditions according to the needs of the PVT collector. Regarding the testing protocols for the assessment of the electrical properties, the international standard IEC 62108:2016 has been employed.

The aim is to test the CPVT solar collector for its overall electrical and thermal parameters and evaluate its performance. The tests have been performed at both the Solar Laboratory of the University of Gävle (stated in the manuscript as HiG) in Gävle (Sweden) during the summer months and at the certification Solar Keymark facilities of the Solar & Energy Systems Laboratory (SESL) from the National Centre for Scientific Research of Demokritos (stated in the manuscript as NCSRD) campus (latitude/longitude: $+37^\circ\ 58'/-23^\circ\ 43'$) during the period of September-October.

2.3.1. Testing facilities and procedure description for Gävle, Sweden

To reduce the size of the manuscript and to avoid repetition, both the schematic and experimental setup (technical drawing scheme from the Swedish testing facility, respectively), as well as the methodology employed to access both electrical and thermal measurements which measure inlet, outlet and ambient temperature, pressure, flow rate, and global and diffuse solar radiation has been presented and detailed by Cabral (2022). Therefore, the following description of the testing facilities comprises only the NCSRD testing site in Athens (Greece), which only differs from Cabral (2022) on the solar collector testing stand automatic/manual operation mode while measuring the IAM factor coefficient.

2.3.2. Description of the testing facilities - Greece

The test bench of the PVT collector includes a two-axis automated tracker, a temperature preparation unit (includes an air-source HP and a storage tank) and a pumping station for adjusting the temperature of the HTF and fixing the flow rate equipped with several pneumatic valves and mixing circuits. The tracker is shown on the left of Fig. 1, while the test loop is presented on the right of Fig. 1.

The collector has been mounted and fastened on the tracker with the inlet and outlet pipes (from one side of the collector) connected to the pumping station. A U-tube has been placed at the piping at the left part of the collector and then insulated, as shown at the left of Fig. 2. Temperature sensors (i.e., PT100) have been installed at the inlet/outlet piping of the collector to measure the water/glycol temperature, as shown at the right. These piping parts have been insulated, once the charging and venting processes have been accomplished, as shown in Fig. 2.

The system has been charged with a water/glycol mixture, in which an antifreeze Tyfocor L[1 and 2] that has antioxidant additives and protects the aluminium receiver from oxidation has been used with a concentration of 40%$_{vol}$. The inlet/outlet piping near the collector was then insulated and the electrical wiring connected with the IV tracer at the back of the stand (Fig. 3) for measuring the power at maximum power point tracking (MPPT).

3. Testing parameters and procedure

Several sets of outdoor tests to acquire various solar collector parameters have been performed, such as a collector electrical and thermal performance test at tracking mode, in which the incidence angle does not affect the results (e.g., whenever the solar irradiation is perpendicular to the solar collector surface plane). The detailed testing parameters can be found in Annex A.

It is important to state that testing standards measurement methods are designed to be replicable (e.g., provide the same results) for any weather conditions and pilot locations. Moreover, the testing standards are based on $\Delta T = T_{collector} - T_{ambient}$ and Solar irradiance, the latter to be from 0 up to 1100 W/m^2, meaning that both ISO and IEC testing standards are not site-dependent and thus ideal for the comparison that the authors want to achieve.

3.1. Measurement sensors

All temperature/fluid sensors and flow meters that have been used have been calibrated and are shown in the following Table 2, providing the measurement range as well as their accuracy. The processing of the results has been conducted based on the density and specific heat capacity of the water mixture, according to its properties as a function of concentration and temperature. For that purpose, a regression analysis and the fitting combined with a statistical analysis concluded polynomial correlations.

3.2. Thermal performance tests

During all these tests, the flow rate has been fixed at 0.02 kg/s/m^2, which represents 3.2 lt/m. This flow rate slightly changes during the tests, due to the variation of the temperature of the water/glycol mixture, but without affecting the performance curves. After that, the performance tests in tracking mode were performed. Once the local weather forecast gave allowed a completely clear sky day with low/moderate wind speed, the collector was uncovered from early in the morning throughout the day while the tracker was continually moving to follow the sun's path (Fig. 4).

The pyranometer is placed on the tracker, at the same solar collector plane, and always records the incident global solar irradiation, while the pyranometer for diffuse radiation is satellite-driven and automatically adjusts its position to align the shadow ring accordingly. The difference between both pyranometers provides direct irradiation on the tilted collector surface. In addition to the solar radiation measurements, the ambient air temperature was also measured, as well as the inlet/outlet fluid temperatures and the flow rate of the water/glycol mixture.

The sampling rate of all measurements is 1 min. Once the thermal properties of the collector have reached a steady-state condition, the electrical measurements took place, with the use of an IV tracer, to calculate the maximum power (MPPT) of each of the PV strings. The heat production per m^2 of the collector is described by Eq. (1) (Nasseriyan et al., 2020).

$$P_{th} = P_{th,\exp} - P_{th,loss} \tag{1}$$

where $P_{th,\exp}$ is the exploitable thermal power, and $P_{th,loss}$ are the thermal losses of the collector. The heat produced (exploitable thermal power) per m^2 of collector surface is given by Eq. (2) (Skoplaki and Palyvos, 2009).

$$P_{th,\exp} = n_{th,b} \bullet I_{b,T} \bullet IAM_{th} + n_{th,d} \bullet \left(I_{d,T} + I_{ref,T}\right) \tag{2}$$

whereas the thermal losses per m^2 are given by Eq. (3) and presented in Lämmle et al. (2017).

$$P_{th,loss} = a_{th,1} \bullet (t_m - T_a) + a_{th,2} \bullet (t_m - T_a)^2 \tag{3}$$

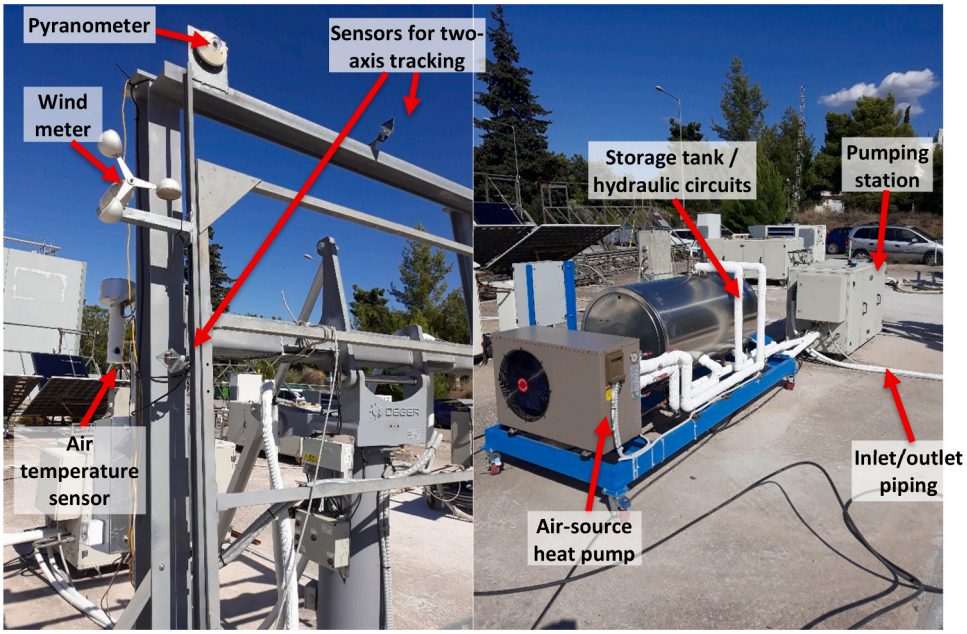

Fig. 1. Two-axis tracker (i.e., left side) and water preparation unit with the pumping station (i.e., right side).

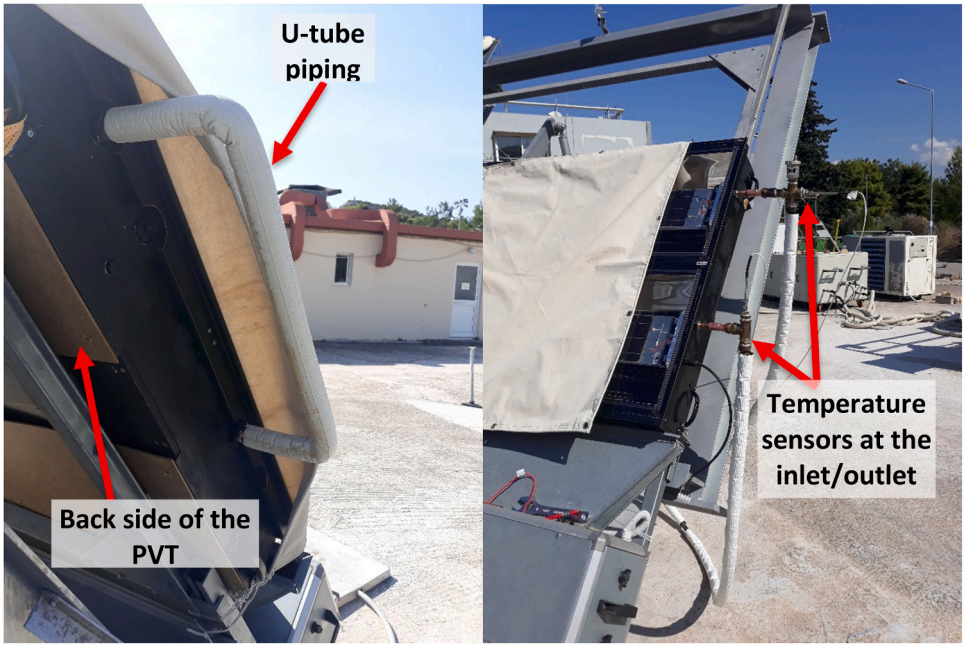

Fig. 2. Inlet/outlet piping installation with temperature sensors and u-tube at the left part of the collector.

Fig. 3. PVT collector mounted at the tracker and charged with water/glycol.

Eq. (1) then provides the heat gain, which is equal to the heat absorbed by the circulated solar fluid, as shown in Eq. (4) and presented in Tzivanidis et al. (2015).

$$P_{th} = n_{th,b} \bullet I_{b,T} \bullet IAM_{th} + n_{th,d} \bullet \left(I_{d,T} + I_{ref,T}\right) - \left[a_{th,1} \bullet (t_m - t_a) + a_{th,2} \bullet (t_m - t_a)^2\right]$$

$$= \dot{m}_{PVT} \bullet c_{p,PVT} \bullet \left(t_{PVT,out} - t_{PVT,in}\right)/A \quad (4)$$

where $\dot{m}_{PVT}$ is the mass flow rate of the water/glycol mixture, $c_{p,PVT}$ is its specific heat capacity, $t_{PVT,out}$, $t_{PVT,in}$ are the outlet and inlet fluid temperatures from the collector, respectively, and A is the gross PVT collector surface area. The water/glycol mixture circulating in the PVT

Table 2
Sensors and meters of the collector stand.

	Sweden		*Greece*	
Thermal measurement equipment	*Measurement range*	*Accuracy*	*Measurement range*	*Accuracy*
Flow rate $\dot{m}$ [L/m]	Up to 10	±1.5%	Up to 17	< 1%
Temperature interval ΔT [°C]	Up to 90	±0.04%	Up to 100	-
Pressure interval ΔP [Bar]	Up to 6	±1.5%	-	-
Heater [°C]	10-90	±0.04%	-	-
Wind Speed [m/s]	-	-	Up to 50	< 2%
Pressure transmitter [Bar]	6	±1%	-	-
Electrical measurement equipment	*Measurement range*	*Accuracy*	*Measurement range*	*Accuracy*
Pyranometer CMP3 (diffuse radiation) [W/m^2]	Up to 2000	±1.5%	-	-
Pyranometer CMP6 (global radiation) [W/m^2]	Up to 2000	±1%	-	-
Pyranometer CMP11 (diffuse radiation) [W/m^2]	-	-	Up to 4000	±1.3%
Pyranometer CMP11 (global radiation) [W/m^2]	-	-	Up to 4000	±1.3%
IV Tracer [V_{oc} - V]	Up to 1000	0.1%	Up to 1000	≤ 0.5%
IV Tracer [I_{sc} - A]	Up to 15	0.1%	Up to 15	≤ 1%

circuit has a high concentration of glycol with anticorrosive additives to protect the aluminium receiver of the PVT collector. The glycol selected is Tyfocor L.[1] Its concentration is 40%$_{vol}$ (for a minimum of around 30%) and the mixture properties (density and specific heat capacity) are given as a function of concentration and temperature from the available dataset provided by the manufacturer.[2]

In the previous equations, $I_{b,T}$, $I_{d,T}$ and $I_{ref,T}$ are the hourly beam (direct), diffuse and reflective radiation components on the tilted collector surface, respectively, expressed in W.m^2. Moreover, t_m [°C] is the mean water temperature in the PVT collector and t_a is the ambient temperature.

The thermal efficiency coefficients $n_{th,b}$ and $n_{th,d}$ correspond to heat acquisition by beam and diffuse irradiation, respectively. The thermal loss parameters $a_{th,1}$ and $a_{th,2}$ (Eq. 3) are characteristic of the collector. Finally, IAM_{th} is the thermal incidence angle modifier, whereas the thermal efficiency of the PVT collector (n_{th}) is defined by Eq. (5) (Gorouh et al., 2022).

$$n_{th} = \frac{P_{th}}{G_T} \tag{5}$$

where $G_T = I_{b,T} + I_{d,T} + I_{ref,T}$ is the global incidence radiation on the tilted collector surface (Duffie and Beckman, 2013). The electrical production per m^2 of the PVT collector is given by Eq. (6), and the electrical efficiency (n_{el}) by Eq. (7) (Cabral and Karlsson, 2018).

$$P_{el} = \left[n_{el,b} \bullet I_{b,T} \bullet IAM_{el} + n_{el,d} \bullet \left(I_{d,T} + I_{ref,T}\right)\right] \bullet \left[1 - a_{el} \bullet \left(t_m - t_{stc}\right)\right] \tag{6}$$

$$n_{el} = \frac{P_{el}}{G_T} \tag{7}$$

where t_{stc} is the standard temperature at test conditions of 25 °C, $n_{el,b}$ and $n_{el,d}$ are the electrical efficiency coefficients that correspond to electrical production at beam and diffuse irradiation, respectively, and a_{el} is the temperature loss coefficient. The quantities $n_{el,b}$, $n_{el,d}$ and a_{el} are characteristic of the PVT collector. Finally, IAM_{el} is the electrical incidence angle modifier, which is discussed later. Efficiencies of PVT collectors are usually measured while solar beams fall perpendicular to the collector surface. However, the energy absorbed by both the thermal receivers and PV cells at different angles of incidence varies, therefore, the overall solar collector efficiency varies accordingly to its IAM factor

Fig. 4. Left: Pyranometer for diffuse radiation placed next to the stand. Right: Testing of the collector started early in the morning.

[1] Tyfocor L: https://tyfo.de/en/produkt/tyfocor-l/.
[2] Tyfocor L technical information: https://tyfo.de/downloads/TYFOCOR-L_en_TI.pdf.

coefficient. Moreover, by adding up both Eqs. (5) and (7) it is possible to assess the overall efficiency of a PVT solar collector (Shakouri et al., 2022).

3.3. Thermal performance - Heat loss coefficient (U-value) and optical efficiency

As there is no direct orientation from certified bodies regarding the performance assessment of PVT solar collectors, typically, this technology is tested according to the international standard for solar thermal collectors ISO 9806 and the electrical performance according to IEC standards (Jonas et al., 2019).

For solar collector certification purposes, the Solar Keymark certification must be followed, which is described in Annex P5.1 of the Solar Keymark Scheme Rules (SKN, 2019).

For a working fluid temperature variation within relatively small limits, the system can be satisfactorily simulated using the average operating temperature, thus making the comparison between different collectors more straightforward, as no system effects are included (Adsten et al., 2005). The test results have been then processed, to calculate the constant parameters of the collector performance equations for different thermal parameter assessments. Such equations of the highest degree are presented in the following Eqs. (8–10) (ISO, 9806:, 2017).

$$\dot{Qth} = \eta 0,b\cdot(K\theta,b(\theta L,\theta T)Gb + K\theta,d \cdot Gd) - a1\cdot (tm - ta) - a2\cdot (tm - ta)2 - a8\cdot (tm - ta)4 \quad (8)$$

$$Qth = \eta 0,b\cdot (K\theta,b(\theta L,\theta T)\cdot Gb + K\theta,d\cdot Gd) - a1\cdot (tm - ta) - a2\cdot (tm - ta)2 \quad (9)$$

$$Qth = \eta 0,b\cdot (K\theta,b(\theta L,\theta T)\cdot Gb + K\theta,d\cdot Gd) - U \cdot (tm - ta) \quad (10)$$

where $\dot{Q}_{th}$ is the heat gain as calculated by the test data, A_g is the gross area, $n_{0,b}$ and $n_{0,d}$ are the performance parameters for beam and diffuse radiation (defined through this process), $K_{\theta,b}$ and $K_{\theta,d}$ are the incident angle modifiers for beam and diffuse radiation, G_b and G_d are the beam and diffuse radiation on the collector surface, a_1, a_2, and a_8 are the loss parameters (defined through this process), T_m is the mean collector temperature, and T_a is the ambient temperature.

The above equation can be simplified in case the parameters a_2 and a_8 are very small and lower than three times the standard deviation. If only a_8 has a small value, the result is a 2nd-order equation.

According to the order of each equation, the specific heat gain is given by Eq. (10), respectively, once the incident angle modifiers have been set to unity, which is valid for the collector at tracking mode.

The values of the parameters for each equation (1st, 2nd, and 4th order), which come from the processing of the test data, are presented in Table 3, along with their standard deviations, for both testing sites, in Greece and Sweden. These parameters are based on the gross area of the collector.

According to ISO (9806): (2017), for a parameter to be statistically significant, the value must be positive and greater than three times its standard deviation. Based on this, the 4th-order equation includes a negative a_2 value, which does not have a physical meaning, and on top of that the standard deviation of this parameter is about the same as its value. Typically, the coefficient a_8 for concentrator collectors is set to zero accordingly to ISO (9806): (2017), which is in line with the value that was achieved.

Additionally, the $\eta_{0,hem}$ obtained for Sweden is higher than for Greece, but on the other hand, the heat loss coefficients are higher, which evens the results. Therefore, the most suitable equation to translate the thermal performance of the CPVT solar collector is the 2nd order equation, which holds a good accuracy over the whole range of tested temperatures, from the ambient up to 80 °C (Table 4).

Moreover, the thermal peak power of the collector reached 1332 and 1305 W, for Greece and Sweden, respectively, which presents a relative difference of $2\%_{rel}$.

3.4. Incidence angle modifier

The incidence angle modifier (IAM) quantifies these efficiency changes as a function of the solar irradiation incidence angle and the location, azimuth angle and slope of the collector surface.

Except from the above-mentioned performance tests that have been conducted in tracking mode, the tracker has been also used to position the collector to specific incidence angles, corresponding to several transversal and longitudinal angles, and thus identify the IAMs at both directions, which differs for the testing method that has been used in Sweden, where a non-automatic-tracking solar system was used. This way the IAMs were assessed in two different ways, to demonstrate that non-automatic-tracking systems are as reliable as a two-axis tracking system if the testing procedure is to be followed to the full extent.

Once the performance parameters of the collector have been fixed with the 2nd order equation, in which all IAM values are equal to 1, the so-called IAM tests have been performed during another clear day, when the position of the collector was manually varied, to follow the sun movement, and keep either a transversal angle equal to zero or the longitudinal angle.

This process requires precise control of the collector positioning, to ensure that a SS thermal condition is reached. Therefore, this kind of test could be done only during the noon hours, when the solar angle and irradiation are constant for a duration from 2 to 3 h, which is adequate to reach a steady-state condition. Another way of testing IAMs is to test the solar collectors during a range of days around the equinoxes as the projected south-angle is fairly constant throughout the days, which leads to fewer correction factors and errors, as only one direction needs to be shifted, either the longitudinal direction or the transversal direction.

Moreover, for each angle that was swept, the other angle was kept equal to zero. Thus, the pairs of transversal/longitudinal angle modifiers

Table 3
Parameter values and standard deviation of the performance correlation of the PVT collector.

Greece - 1st Order		St. dv.	Units
$\eta_{0,hem}$	0.515	0.004	-
U_0	4.422	0.14	W/m^{2}K
Sweden - 1st Order		**St. dv.**	**Units**
$\eta_{0,hem}$	0.524	0.009	-
U_0	4.517	0.17	W/m^{2}K
Greece - 2nd Order		**St. dv.**	**Units**
$\eta_{0,hem}$	0.505	0.004	-
a_1	3.216	0.371	W/m^{2}K
a_2	0.021	0.006	W/m^{2}K^2
Sweden - 2nd Order		**St. dv.**	**Units**
$\eta_{0,hem}$	0.513	0.004	-
$\eta_{0,diff.}$	0.504	0.004	-
a_1	3.87	0.433	W/m^{2}K
a_2	0.026	0.01	W/m^{2}K^2
Greece - 4th Order		**St. dv.**	**Units**
$\eta_{0,hem}$	0.510	0.005	-
a_1	4.536	0.7	W/m^{2}K
a_2	-0.028	0.024	W/m^{2}K^2
a_8	0.000009	0.000004	W/m^{2}K^4

Table 4
Thermal peak performance parameter values and respective HTF temperatures of the PVT collector.

	Thermal peak efficiency [%]	Thermal peak power [W/m^2]	t_m [°C]
Greece	51.5	579	26
Sweden	52.1	567	24

obtained are: [0°-30°], [0°-40°], [0°-50°], [30°-0°], [40°-0°], and [50°-0°]. For estimating the electrical IAMs, another angle of 15° has been obtained for both directions [0°-15°] and [15°-0°].

The IAM tests have been conducted during October, following the testing procedure previously described. The thermal performance should be stabilized and reach a steady-state condition for 10 min, with the recorded test data during that period to be further processed.

The thermal IAMs can be calculated via Eq. 11, which is based on the test data. The specific heat capacity c_p and the density used to calculate the mass flow rate $\dot{m}$ correspond to the water/glycol mixture at the mean HTF temperature (ISO, 9806:, 2017).

$$K_b(\theta) = \frac{\frac{\dot{m} \bullet c_p \bullet (T_o - T_i)}{A_g} + \alpha_1 \bullet (t_m - t_a) + \alpha_2 \bullet (t_m - t_a)^2}{G \bullet \eta_{0,hem}} \quad (11)$$

Finally, the diffuse incidence angle modifier constant (K_d) can be retrieved by the following Eq. 12.

$$K_d = \frac{1}{C_i} \quad (12)$$

For a given set of data points retrieved from the measurements on the CPVT solar collector, the diffuse incidence angle modifier constant K_d was found to be 0.72, which shows that the overall solar collector theoretical K_d of 0.77, in reality, is lower, which leads to a higher overall C_i than the overall solar collector concentration ratio of 1.3.

The measured K_d of 0.72 shows that the top reflector part that is above the axis line of the receiver contributes to increase the overall concentration ratio, providing some extra sunlight to the top receiver side, which leads to an overall solar collector measured concentration ratio of ~1.38 suns.

Moreover, the IAM profile for both heat and electricity production is different, which expresses the variance in output performance of a PVT collector as the angle of incidence of the sun changes with the solar collector surface plane. A transversal, θ_T, and a longitudinal, θ_L, incidence angle is calculated by Eqs. (13) and (14), respectively.

$$\theta_T = \tan^{-1}[\tan\alpha \bullet \cos(\Phi - \gamma)] - \beta \quad (13)$$

$$\theta_L = \tan^{-1}\left[\frac{\sin\alpha \bullet \sin(\Phi - \gamma)}{\cos\vartheta}\right] \quad (14)$$

where α, Φ and ϑ are the solar height, azimuth and incidence angle, respectively, which change over time both during the day and during the year. Moreover, γ is the azimuth and β is the slope of the PVT collector, which depends on the installation of the collector.

The transversal and longitudinal IAM for each case, i.e. thermal or electrical, are based on the angles θ_T and θ_L given from Eqs. (13) and (14), respectively. The total IAM is then given by Eq. (15) as the product of the transversal with the longitudinal IAM.

$$IAM = IAM_{tran} \bullet IAM_{long} \quad (15)$$

From the test method described for both transversal and longitudinal electrical IAM, the following section presents an analysis of the results obtained for the electrical $IAM_{Long.}$ and IAM_{Transv}. The normalized IAM factor (for normal incidence) has been acquired by the relation between several parameters, such as the angle of incidence, global irradiation and electrical power.

4. Testing results

4.1. Incidence angle modifier

4.1.1. Electrical incidence angle modifier

Following the previous statements, the following Figs. 5 and 6 present the outdoor testing results for both testing sites, regarding the longitudinal and transversal electrical IAM, respectively.

The longitudinal electrical IAM has a smooth pattern, due to the opening in section A of the DM geometry. Furthermore, the RES4BUILD is not dependent on the solar collector tilt angle as it can be placed as a standard PV module. Moreover, the acceptance angle (around 21° ± 1°) of the RES4BUILD solar collector is well defined in Fig. 5. Differences of up to 2% (Table 5) have been registered from both testing sites, which presents a very good agreement between both automated and manual tracking solar stands.

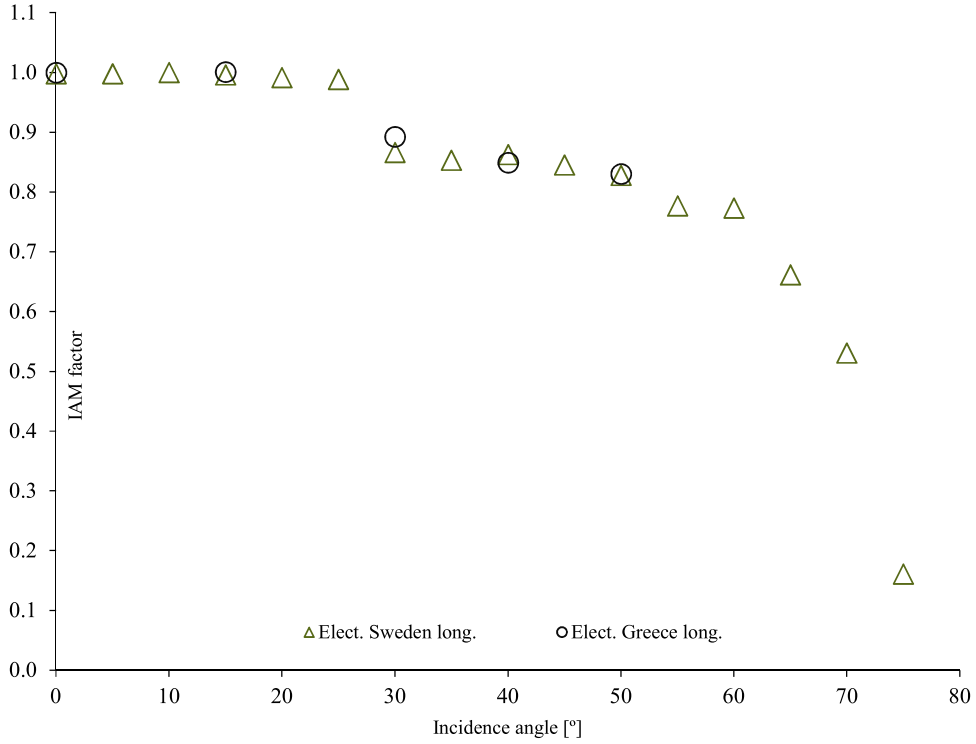

Fig. 5. Longitudinal electrical Incidence Angle Modifier.

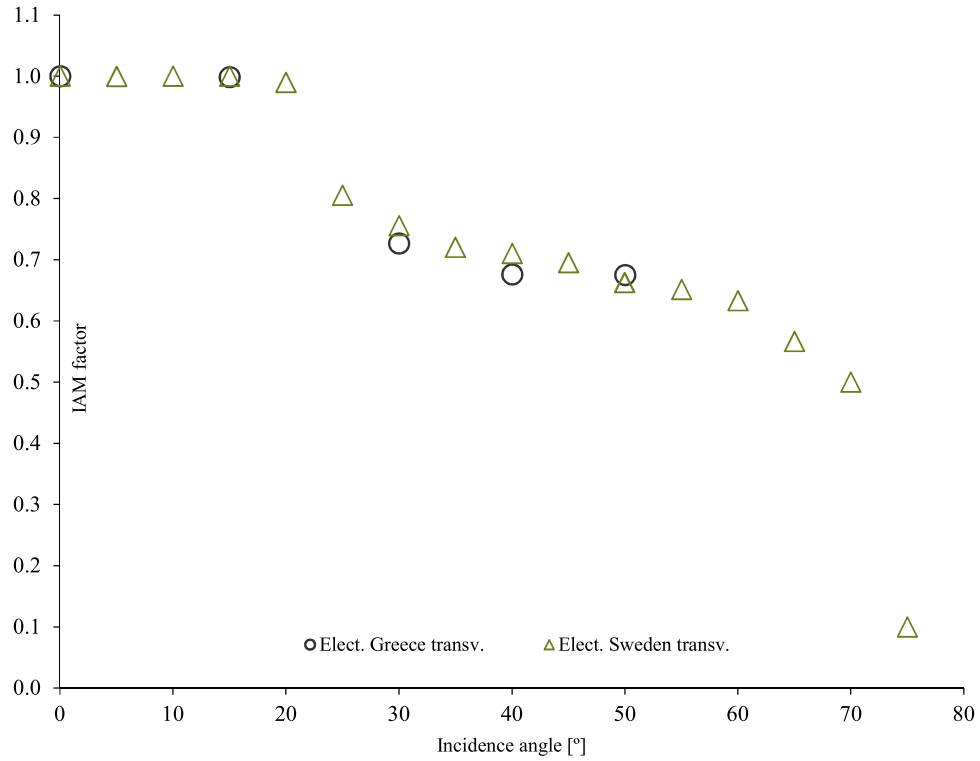

Fig. 6. Transversal electrical Incidence Angle Modifier.

Table 5
Differences in the IAM results for the longitudinal electrical IAM, for both locations: Greece and Sweden.

Angle of Incidence [º]	$IAM_{Long.}$ – Greece [%]	$IAM_{Long.}$ – Sweden [%]	Difference [%]
30	89	87	~2
40	85	86	~1
50	83	83	~0

Additionally, the transversal electrical IAM has been measured and a comparison between both testing results from Greece and Gävle are presented in the following Fig. 6.

Furthermore, it is possible to visualize the importance of the diode system and the PV cell string layout in the overall performance of a PV system. Fig. 6 clearly shows at which angle of incidence the diode system kicks in, which is around 21 ± 1º, where a significant decrease in efficiency is presented. Differences from 2–3% (Table 6) have been registered from both testing sites, which presents a very good agreement between both automated and manual tracking solar stand systems.

The marginal variances observed lack significance since the discrepancies leading to a decline in energy production in the annual evaluation are confined to specific angles of incidence. These differences do not extend across a broad range of angles, which would undoubtedly have a substantial impact on the overall yearly electricity generation.

Table 6
Differences in the IAM results for the transversal electrical IAM, for both locations: Greece and Sweden.

Angle of Incidence [º]	$IAM_{Transv.}$ – Greece [%]	$IAM_{Transv.}$ – Sweden [%]	Difference [%]
30	73	76	~4
40	68	71	~4
50	68	66	~3

4.1.2. *Thermal incidence angle modifier*

Additionally, the test method previously described has been applied to access the thermal IAM, which is presented in the following section. The normalized IAM factor (for normal incidence) has been acquired by the relation between several parameters, such as the angle of incidence, global irradiation and electrical power. Furthermore, the following Fig. 7 presents the outdoor testing of the longitudinal thermal IAM for both testing locations.

The reflective gables were expected to decrease slightly the longitudinal IAM since no light will go through at incident angles higher than + 45º. On the other hand, this penalty in performance will not affect significantly the performance at the relevant incident angles between 0º and + 45º. Differences from 2–5% (Table 7) have been registered from both testing sites, which presents a very good agreement between both automated and manual 2-axis tracking solar stands.

Additionally, the transversal direction impact on the thermal $IAM_{transv.}$ is major in relation with the longitudinal thermal IAM, as can be seen in the following Fig. 8.

As expected, the thermal $IAM_{transv.}$ has a steadier pattern than the electrical $IAM_{transv.}$ due to its physical characteristics (e.g., a broader range of the solar radiation spectrum). Differences from 1–5% (Table 8) have been registered from both testing sites, which presents a very good agreement between both automated and manual 2-axis tracking solar stands. Nevertheless, the deviation that occurred at 30º presents a misalignment from the Swedish testing site, as, the deviations presented in the previous IAM testing results tend to increase for higher angles of incidence.

On the other hand, the theoretical acceptance half-angle being 21 ± 1º allows the reader to conclude that the thermal capacity of the collector is of interest, (i.e., therefore presented in chapter 4.3) as it takes longer to decrease in efficiency as it takes some time to cool down the receiver (e.g., the difference between 20º and 30º is negligible) and thus allowing the extraction of more thermal power.

As stated for the electrical IAM, the marginal disparities highlighted hold even less relevance for the thermal IAMs, as the noted variations causing a decrease in thermal energy production during the annual

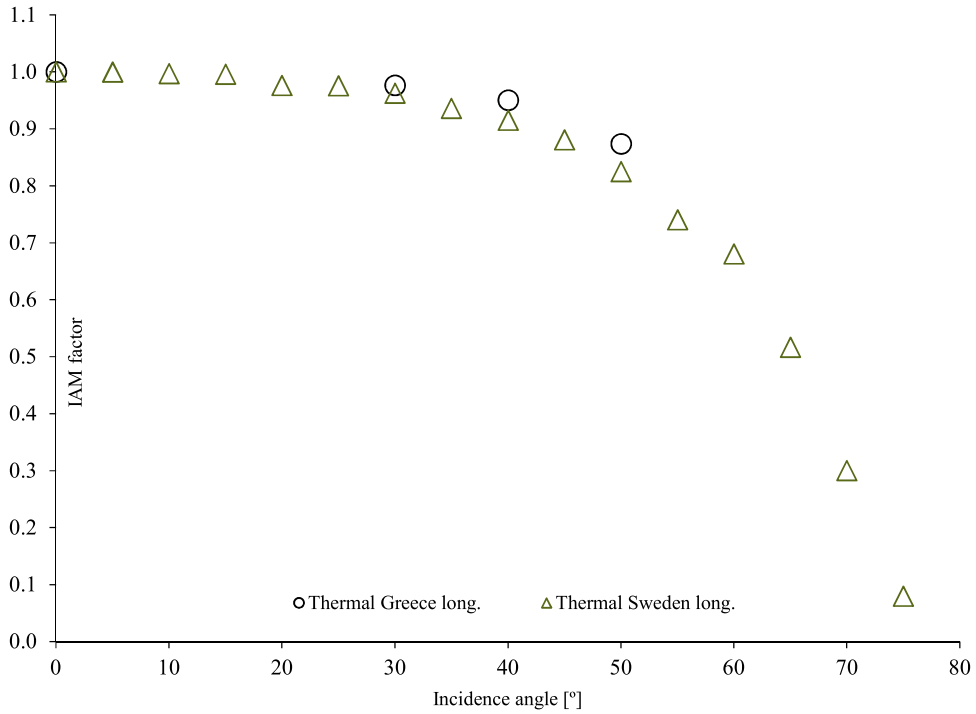

Fig. 7. Longitudinal thermal Incidence Angle Modifier.

Table 7
Differences in the IAM results for the thermal longitudinal IAM, for both locations: Greece and Sweden.

Angle of Incidence [°]	$IAM_{Long.}$ – Greece [%]	$IAM_{Long.}$ – Sweden [%]	Difference [%]
30	98	96	~2
40	95	92	~3
50	87	82	~5

assessment are specific to a limited set of angles of incidence, which would not change the thermal mass value for an yearly evaluation assessment.

4.2. Daily thermal performance tests in stationary mode

All the previous tests are necessary for identifying the performance of the PVT collector for every relative incidence angle. Additional tests have been conducted, to assess the thermal capacity and time constant of the tested CPVT solar collector. During the outdoor tests, the PVT collector was kept at a constant tilt of 40°, facing south (azimuth = 0 °). These tests took place during October with an inlet temperature of 22 °C, on a clear sky day.

The following Fig. 9 presents the relation between the irradiation profiles, the ambient and inlet/outlet temperature in comparison with the heat gains from the solar collector. For better data visualization, the ambient temperature has not been plotted, since during the test procedure, the ambient temperature had a constant increase from 20 °C up to 25 °C throughout the whole day.

Around noon, a rapid variation of the inlet collector temperature has been imposed, to evaluate the step-response of the collector. The maximum temperature difference of the collector is up to 6 °C, with this difference being a good indicator of the heat gain at every step since the water/glycol flow rate is constant. Despite the inlet temperature increase of around 6 °C, the thermal behaviour of the CPVT was not significantly affected as it decreased around 65 W/m^2 and then stabilized at around 535 W/m^2, which provides a good setpoint regarding the thermal capacity of this concentrating solar collector.

The maximum heat gain reached a peak of around 579 W/m^2 (e.g., obtained for a mean HTF temperature of t_m - t_a = 0 K) during the 15th of October in Greece, which can then be directly compared with two more days, with similar radiation profiles but with different intensities, both in Greece and Sweden, as can be seen in the following Table 9.

As expected, the thermal peak power is directly influenced by the solar radiation intensity and HTF mean temperature, as well as the ambient temperature. Both days, 25/06 and 15/10, have similar ambient and HTF mean temperatures, which can be translated into similar thermal energy production, however, the solar radiation intensity is fairly diverse, which leads to dissimilar thermal outputs and therefore different daily mean thermal efficiencies.

For higher temperatures, this efficiency drops significantly, which is why a solar buffer tank should be added together with the solar collector, to be charged with low-temperature heat, especially during winter.

4.3. Effective thermal capacity and time constant (dynamic response tests)

Moreover, to assess the effective thermal capacity, the solar collector area is shielded from solar radiation through a solar reflecting cover. The inlet HTF temperature is set to close to the ambient temperature until SS conditions are met, which means that the outlet HTF temperature should be similar to the inlet HTF temperature. The cover is then quickly removed, and data are measured until the outlet temperature of the fluid varies by less than 0.5 K/min (i.e., until SS conditions are met).

The transient behaviour of the collector between the two SS conditions, once covered and fully operational, can be described by the following Eq. (16) (Fischer and Müller-Steinhagen, 2009).

$$C\frac{dT}{dt} = A.\eta_{0,hem}.G - \dot{m}.c_f dT - A_G.U.(T_m - T_a) \quad (16)$$

The effective thermal capacity C is then calculated from the measurement data points of the inlet and ambient temperature, and the incidence solar irradiation. Integrating over the period between the two

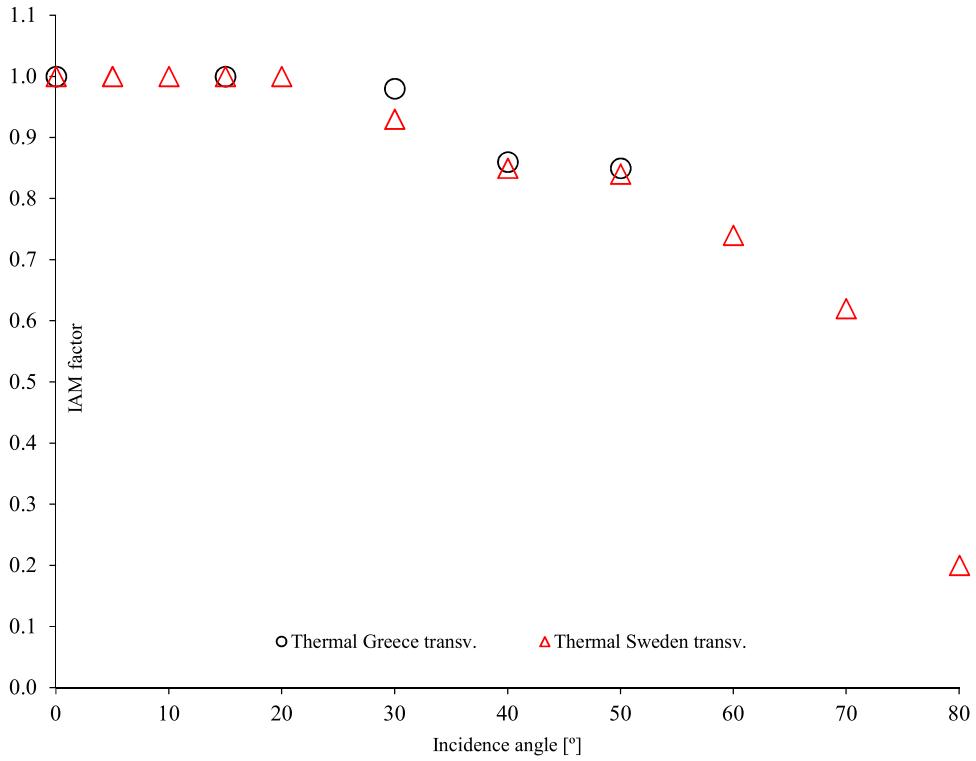

Fig. 8. Transversal thermal Incidence Angle Modifier.

Table 8
Differences in the IAM results for the thermal transversal IAM, for both locations: Greece and Sweden.

Angle of Incidence [º]	$IAM_{Transv.}$ – Greece [%]	$IAM_{Transv.}$ – Sweden [%]	Difference [%]
30	98	93	~5
40	86	85	~1
50	85	84	~1

steady-state conditions (from t_1 to t_2) it is possible to retrieve the solar collector's effective thermal capacity, by applying the following Eq. (17) (ISO, 9806:, 2017).

$$C = \frac{A.\eta_{0,hem}\int_{t1}^{t2} G dt - \dot{m}.c_f.\int_{t1}^{t2} dT dt - A_G.U.\left[\int_{t1}^{t2}(T_{in}-T_a)dt + \frac{1}{2}\int_{t1}^{t2} dT dt\right]}{T_{m2}-T_{m1}} \quad (17)$$

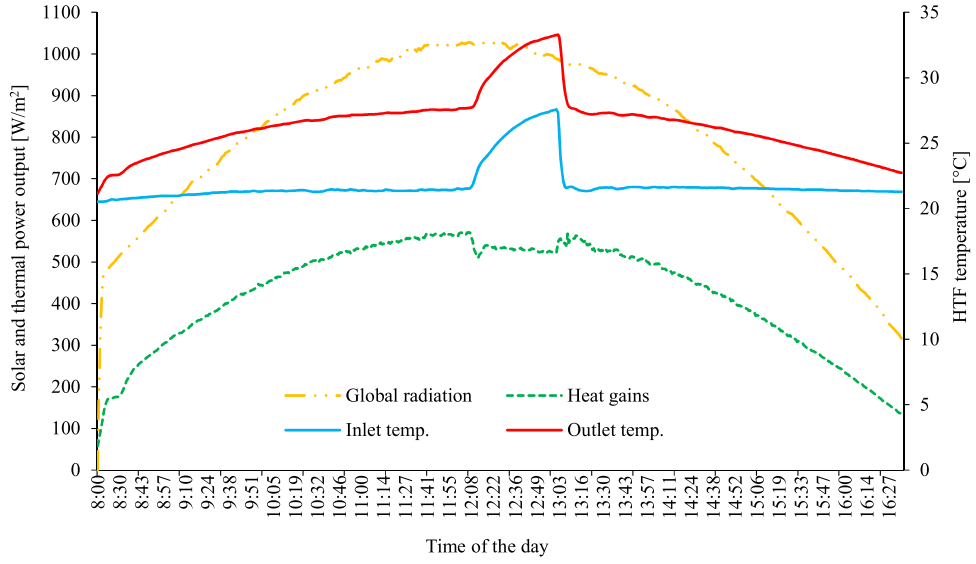

Fig. 9. Inlet/outlet temperatures at the collector, solar radiation and ambient temperature during the 15th of October.

Table 9
Daily peak thermal energy for three different days, both in Sweden and Greece.

Location / Day	Daily thermal energy [kWh/day]	Daily average mean temperature [°C]	Daily global solar irradiation [kWh/day]	Average daily thermal efficiency [%]
Sweden 25/06	10.3	23.5	18.8	54.9
Greece 15/10	8.2	24.1	15.4	52.9
Greece 20/10	6.0	28.7	12.6	47.5

The effective thermal capacity of the PVT collector reached the value of 63.24 kJ/K, which is in line with the typical values registered by ST collectors.

4.4. Time constant

During the same testing procedure, the time constant (τ_c) can also be retrieved, which is defined as the elapsed time between the removal of the cover/shield and the moment when the collector outlet temperature crosses 0.632 of the total increase from one steady-state condition ($T_{out} \sim T_{amb}$) to the normal steady-state operation.

The time needed for the collector to reach this temperature has been calculated based on the testing procedures presented under the standard ISO (9806): (2017) and has been found as $\tau_c = 124$ s, which is also in line with the typical values registered by ST collectors.

4.5. Electrical performance introduction

The electrical performance of the CPVT collector was characterized according to IEC 62108 (2016) while the thermal performance was characterized according to ISO (9806): (2017) (by Steady-state (SS) test methods). The glazed PVT collectors are not classified as wind and infrared-sensitive collectors (WISC). Therefore, the additional thermal losses due to wind convection and infrared radiation are not considered.

The following section presents different sets of results, such as electrical daily (instantaneous) peak power, optical efficiency and thermal measurements, heat loss coefficient, and both transversal/longitudinal electrical/thermal IAM diagrams.

4.5.1. Daily electrical performance tests at stationary mode

By using active cooling and an improved reflector geometry the electrical performance of the PV cells is expected to improve, due to an increase in the actual electrical peak efficiency. Therefore, a clear sky day in September has been selected to provide a better understanding of the daily electrical performance profile of the CPVT solar collector for both the bottom and top receiver sides. The data has been collected for a whole day in September for a solar collector tilt of 61° and a constant HTF temperature of 20 °C. The ambient temperature reached as high as 15 °C and it is presented in the following Fig. 10.

For a module temperature of 25 °C, an electrical peak efficiency of almost 11% can be achieved, nevertheless, it is known that module temperature tends to be lower than the actual PV cell temperature, which provides a good insight that if the PV cell temperature is to be 25 °C, the electrical peak efficiency it would be higher.

Reflection and absorption losses, together with mismatches in the manufacturing processes (e.g., physical gap between PV cells) increase the 'dead' area, leading to lower electrical outputs. Manufacturing processes require constant refinements, as typically the PV cell connection increases resistance losses, even if all the cells are theoretically batched together into power bands, it will not match perfectly and bring to light the electrical performance of the lowest current generated for a single PV cell within the PV cell substring.

Moreover, at tracking mode, when the effect of the IAMs is negligible (e.g., equal to unity), the electricity production has been measured with an IV tracer, which adjusts the voltage and current, to identify the condition with the maximum electrical power production.

This measurement tends to be very fast (e.g., just a few seconds are required) and is conducted once the thermal performance has reached a steady-state condition. The whole IV curve is swept by the tracer and the MPPT point is then identified. This process is repeated for all the solar collector troughs. The results at tracking mode are plotted in the following Fig. 11.

The measurements for a mean collector temperature of 26 °C have been conducted twice, to increase the accuracy of the data, since the electrical peak power is defined as the temperature at standard testing conditions (STC) of 25 °C. The summary of the electrical peak performance parameters and respective HTF temperatures of the PVT collector, for both locations, is presented in the following Table 10.

The total solar collector power output reached 1550 W in Greece and

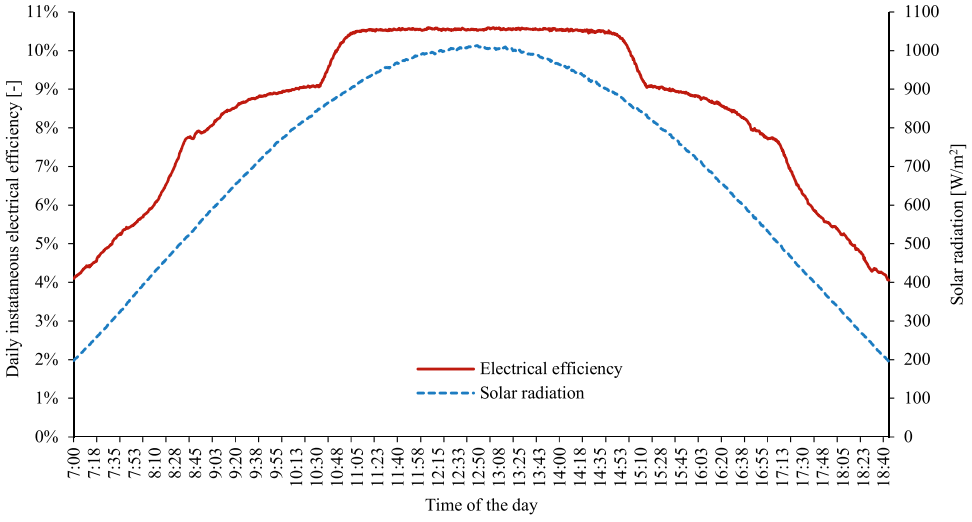

Fig. 10. Electrical daily instantaneous efficiency and solar radiation profile for a clear sky day.

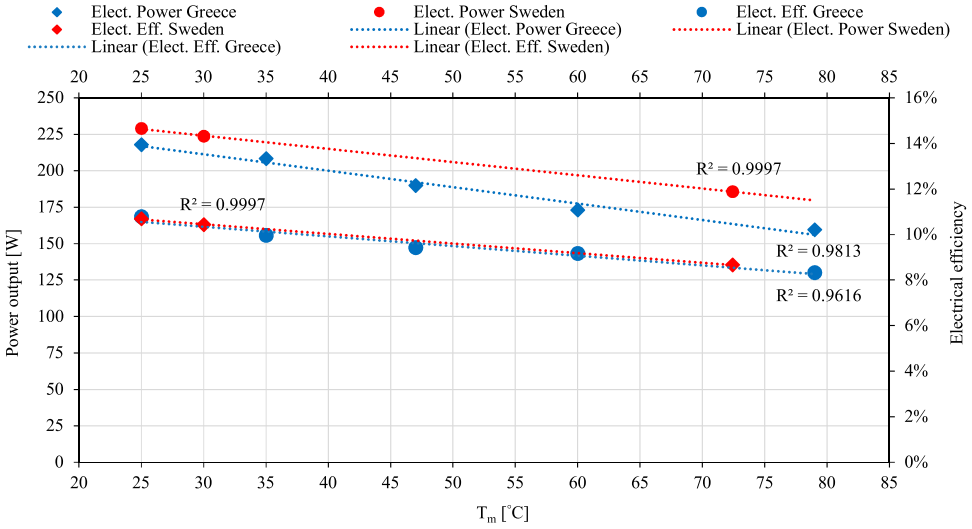

Fig. 11. Electrical peak performance efficiency and power trend in relation with the solar collector HTF temperature.

Table 10
Electrical peak performance parameter values and respective HTF temperatures of the PVT collector, for both locations: Greece and Sweden.

	Electrical peak efficiency [%]	Electrical peak power [W]	Solar radiation intensity [W/m^2]	T_m [°C]
Greece	10.8%	218	878	26
Sweden	10.7%	229	931	24

1534 W in Sweden, which can be translated to 674 and 667 W/m^2, respectively for Greece and Sweden, which leads roughly to a minor difference of 1%.

5. Conclusions

Automated two-axis tracking systems consistently surpass manual counterparts in terms of precision and energy capture efficiency, especially when integrated into optimal scenarios like large-scale solar farm setups where optimizing energy generation holds paramount importance.

Conversely, manual two-axis tracking solar systems retain viability in specific contexts, as expounded in this manuscript. These systems are characterized by simplicity, cost-effectiveness, suitability for smaller installations and off-grid configurations.

Consequently, an extensive series of outdoor assessments were conducted on a Concentrating Photovoltaic-Thermal solar collector. These tests were carried out on both automated and manual two-axis tracking solar systems, adhering to the standard testing protocols ISO (9806): (2017) and IEC 62108:2016. The evaluations encompassed electrical and thermal performance parameters, alongside the determination of Incidence Angle Modifier coefficients.

The observed divergence in overall peak power performance across test sites was merely 1%, culminating in a maximum of 1550 W_{peak}. This aggregate encompasses an electrical peak capacity of 218 W_{peak}, equating to an electrical peak efficiency of 10.8%, as well as a thermal peak capacity of approximately 1332 W_{peak}, resulting in a thermal peak efficiency of 52%.

Furthermore, the most notable fluctuation encountered in both transversal and longitudinal Incidence Angle Modifier coefficients was confined to a threshold lower than 5%. Consequently, it was feasible to ascertain an acceptance half-angle of 21 $\pm$ 1°.

The innovations in insulation have significantly elevated the comprehensive efficiencies while concurrently mitigating thermal losses. This enhancement has translated into augmented annual energy yields, thereby establishing a second-order thermal peak efficiency of about 52%, accompanied by a heat loss coefficient of 3.87 W/m^2·K and a temperature-dependent coefficient of 0.026 W/m^2·K^2. The marginal differences between IAMs are relatively insignificant, with variations typically falling below 5% for specific angles of incidence. This translates to an even smaller impact on annual electrical and thermal performance assessments.

The minimal discrepancies delineated in this exposition across testing sites underscore the meticulous precision exhibited by both automated and manual two-axis tracking solar system structures when the stipulated testing protocols are diligently adhered to. Thus, during the assessment of the actual necessity for automated two-axis tracking systems to achieve heightened result precision, it is imperative to bring the cost-effectiveness of manual two-axis tracking solar systems to the forefront of deliberation, given the marginal disparities documented in this study.

Furthermore, precision emerges as a pivotal determinant in the efficacy of any two-axis tracking solar systems, with a direct bearing on energy harvesting efficiency. Although automated systems offer superior precision and energy capture potential, manual counterparts retain applicability in specialized domains. Engineers must meticulously evaluate these alternatives based on project and testing requisites, encompassing factors such as scale, budgetary considerations, and maintenance capacities, enabling a judicious choice that optimizes energy production and financial prudence.

CRediT authorship contribution statement

Cabral Diogo Oliveira: Writing – review & editing, Writing – original draft, Visualization, Validation, Supervision, Software, Resources, Project administration, Methodology, Investigation, Funding acquisition, Formal analysis, Data curation, Conceptualization. **Kosmadakis George:** Writing – review & editing. **Mathioulakis Emmanouil:** Writing – review & editing.

Declaration of Competing Interest

The authors declare that they have no known competing financial interests or personal relationships that could have appeared to influence the work reported in this paper.

Data availability

The data that has been used is confidential.

Acknowledgements

This project has received funding from the European Union's Horizon 2020 research and innovation programme under Grant Agreement No. 814865 (RES4BUILD). This output reflects only the author's view. The European Climate, Infrastructure and Environment Executive Agency (CINEA) and the European Commission cannot be held responsible for any use that may be made of the information contained therein.

While this publication has been prepared with care, the authors and their employers provide no warranty with regards to the content and shall not be liable for any direct, incidental, or consequential damages that may result from the use of the information, or the data contained therein. Reproduction is authorised providing the material is unabridged and the source is acknowledged.

Annex A

Testing parameters and procedure.

Several sets of outdoor tests to acquire various solar collector parameters have been performed, such as a collector electrical and thermal performance test at tracking mode, in which the incidence angle does not affect the results (e.g., whenever the solar irradiation is perpendicular to the solar collector surface plane). The detailed testing parameters can be found in Annex A.

To assess different performance parameters, the tests have been conducted at five different temperature levels, starting from the ambient temperature of around 22 °C up to almost 80 °C. This assessment process is accomplished by increasing/decreasing the water mixture temperature for the above-mentioned five temperature levels.

Moreover, these tests were finished once 4 of these 10-minute periods were achieved for each temperature level, with the measurements being further filtered, plotted, and analysed.

During the measurement of the required set points at each temperature level, which was constantly recorded, were posteriorly included in the processing whenever the temperature deviation over a 10-minute spam duration was ≤ 0.1 K. This testing protocol is based on the international testing standard for thermal solar collectors ISO (9806): (2017) specifications, which ensures Steady-State (SS) test conditions and increased reliability.

The next set of tests was intended to measure the solar collector performance at each angle of incidence, which leads to the assessment of both transversal and longitudinal IAM. This process required several hours of testing to achieve steady-state conditions while adjusting the position of the collector with the use of the tracker.

According to the ISO (9806): (2017) standard, an IAM value at one incidence angle is only required, but due to the reflector and the collector design, the measurements have been extended to several IAM data points which were measured, three transversal angles of 30°, 40°, and 50° (for a longitudinal angle of 0°), and another three longitudinal angles of 30°, 40°, and 50° (for a transversal angle of 0°).

The thermal and electrical output has been measured under these conditions, while the electrical output was also measured at an angle of 15° (both transversal and longitudinal).

The final set of tests concerned the testing of the collector at stationary conditions (quasi-steady state tests) facing south (azimuth of 0°) and with a tilt of 40° for a complete day. This requires a clear sky day without clouds, with the tests being cloned twice, one with an inlet temperature of 20 °C (i.e., close to the ambient temperature so that the heat losses are negligible) and another one at 27 °C. During the second day, a rapid variation of the inlet collector temperature has been imposed, to identify the step-response of the collector to sudden changes.

References

Adsten, M., Helgesson, A., Karlsson, B., 2005. Evaluation of CPC-collector designs for stand-alone, roof- or wall installation. Sol. Energy 79 (6), 638–647.

Asfaw, A.H., 2023. Manual tracking for solar parabolic concentrator – For the case of solar injera baking, Ethiopia. Helyyon 9, 12884.

Cabral, D., 2022. Development and performance comparison of a modified glazed CPC hybrid solar collector coupled with a bifacial PVT receiver. Appl. Energy 325, 119653.

Cabral, D., Karlsson, B., 2018. Electrical and thermal performance evaluation of symmetric truncated C-PVT trough solar collectors with vertical bifacial receivers. Sol. Energy 174, 683–690.

Cabral, D., Gomes, J., Karlsson, B., 2019. Performance evaluation of non-uniform illumination on a transverse bifacial PVT receiver in combination with a CPC geometry. Sol. Energy 194, 696–708 https://doi.org/10.1016/j.solener.2019.10.069.

Chakravarty, K.H., Said, M., Chakravarty, H., Alsagri, A.S., Howard, T.J., Arabkoohsar, A., 2022. A review on integration of renewable energy processes in vapor absorption chiller for sustainable cooling. Sustain Energy Technol. Assess. 50, 101822.

Dekkiche, M., Tahri, T., Denai, M., 2023. Techno-economic comparative study of grid-connected PV/reformer/FC hybrid systems with distinct solar tracking systems. Energy Convers. Manag.: X 18, 100360.

Demirdelen, T., Alici, H., Esenboğa, B., Güldürek, M., 2023. Performance and economic analysis of designed different solar tracking systems for mediterranean climate. Energies 16, 4197. https://doi.org/10.3390/en16104197.

Duffie, J.A., Beckman, W.A., 2013. Solar Engineering of Thermal Processes. John Wiley & Sons, New York.

El Hammoumi, A., Chtita, S., Motahhir, S., El Ghzizal, A., 2022. Solar PV energy: from material to use, and the most commonly used techniques to maximize the power output of PV systems: a focus on solar trackers and floating solar panels. Energy Rep. 8, 11992–12010.

Gorouh, H.A., Salmanzadeh, M., Nasseriyan, P., Hayati, A., Cabral, D., Gomes, J., 2022. Thermal modelling and experimental evaluation of a novel concentrating photovoltaic thermal collector (CPVT) with parabolic concentrator. Renew. Energy 181, 535.

IEC 62108, 2016. Concentrator photovoltaic (CPV) modules and assemblies – Design qualification and type approval.

ISO 9806, 2017. ISO 9806:2017 Solar energy - Solar thermal collectors – Test methods.

Jonas, D., Lämmle, M., Theis, D., Schneider, S., Frey, G., 2019. Performance modeling of PVT collectors: Implementation, validation and parameter identification approach using TRNSYS. Sol. Energy 193, 51–64. https://doi.org/10.1016/j.solener.2019.09.047.

Lämmle, M., Oliva, A., Hermann, M., Kramer, K., Kramer, W., 2017. PVT collector technologies in solar thermal systems: a systematic assessment of electrical and thermal yields with the novel characteristic temperature approach. Sol. Energy 155, 867–879.

Nasseriyan, P., Gorouch, H., Gomes, J., Cabral, D., Salmanzadeh, M., Lehmann, T., 2020. Numerical and experimental study of an asymmetric CPC-PVT solar collector. Energies 13, 669. https://doi.org/10.3390/en13071669.

Shakouri, M., Ghadamian, H., Hoseinzadeh, S., Sohani, A., 2022. Multi-objective 4E analysis for a building integrated photovoltaic thermal double skin Façade system. Sol. Energy 233, 408–420.

SKN, 2019. Solar Keymark Scheme Rules. SKN_N0444R1, Edition 2019–03-07. Solar Keymark Network (SKN).

Skoplaki, E., Palyvos, J., 2009. On the temperature dependence of photovoltaic module electrical performance: a review of efficiency/power correlations. Sol. Energy 83 (5), 614–624.

Tajouo, G.F., KApen, P.T., Koffi, F.L.D., 2023. Techno-economic investigation of an environmentally friendly small-scale solar tracker-based PV/wind/Battery hybrid system for off-grid rural electrification in the mount bamboutos, Cameroon. Energy Strategy Rev. 48, 10110722.

Tina, G.M., Scavo, F.B., 2022. Energy performance analysis of tracking floating photovoltaic systems. Heliyon 8 (8), 10088. https://doi.org/10.1016/j.heliyon.2022.e10088.

Tzivanidis, C., Bellos, E., Korres, D., Antonopoulos, K.A., Mitsopoulos, G., 2015. Thermal and optical efficiency investigation of a parabolic trough collector. Case Stud. Therm. Eng. 6, 226–237.

Vargas, A.N., Francisco, G.R., Montezuma, M.A.F., Sampaio, L.P., Acho, L., 2022. Low-cost dual-axis solar tracker with photovoltaic energy processing for education. Sustain. Energy Technol. Assess. 53B, 102542. https://doi.org/10.1016/j.seta.2022.102542.

Zhang, S., Oclon, P., Klemes, J.J., Michorczyk, P., Pielichowska, K., Pielichowski, K., 2022. Renewable energy systems for building heating, cooling and electricity production with thermal energy storage. Renew. Sust. Energy Rev. 165, 112560 (https://ourworldindata.org/energy-productionconsumption. https://energy.ec.europa.eu/. https://tyfo.de/en/produkt/tyfocor-l/. https://tyfo.de/downloads/TYFOCOR-L_en_TI.pdf.).